Mapping topobathymetry at ultra-high spatial resolution using RGB UAV and PlanetScope SuperDove neural network fusion

Antoine Collin [1,2], Laurine Nogue [1,2], Dorothée James [1,2], Coralie Monpert [3], Laetitia Dupuy [2,4], Franck Dolique [2,4]

[1] Coastal GeoEcology Lab, EPHE - PSL, 35800 Dinard, France – (antoine.collin ; laurine.nogue; dorothee.james)@ephe.psl.eu
[2] Laboratory of Biology of Aquatic Organisms and Ecosystems, 35800 Dinard, France
[3] Service Hydrographique et Océanographique de la Marine, 29200, Brest, France – coralie.monpert@shom.fr
[4] Laboratory of Biology of Aquatic Organisms and Ecosystems, 97275 Schœlcher, Martinique, France – (laetitia.dupuy; franck.dolique)@univ-antilles.fr

Keywords: PlanetScope SuperDove, Regression, Neural Network, DJI Zenmuse P1, Martinique, French Overseas.

Abstract

Worldwide coastal areas comprise environmental triple points (air, land and seawater) that cope with coastal risks at unprecedented rates of change. Wind- and wave-related acute hazards add up to the chronic sea-level rise on interface zones that increasingly host human population and assets. Those societal challenges need to be overcome using the most discriminant and finest remote sensors.
We present an innovative two-step methodology to produce an ultra-high spatial resolution (UHSR) topobathymetry using a fusion of a RGB camera mounted on an aerial drone with a multispectral satellite imagery provided with very high temporal resolution. The fusion relied on a DJI Zenmuse P1 (0,08 m pixel size) borne by a DJI Marice 300 RTK, the PlanetScope SuperDove imagery, provided with eight bands at 3 m, and linear or nonlinear (neural network with two hidden layers endowed with three neurons, each) regression. Once the fusion achieved, both topography and bathymetry were mapped using, either the digital surface model (DSM) derived from the drone-derived photogrammetry, or the DSM combined with the UHSR SuperDove imagery. Both datasets served as predictors to model a digital topobathymetric terrain LiDAR response using linear or neural network regression.
The best drone-satellite fusion was completed by the bandwise neural network regression, ranging from R^2_{test} of 0,79 for the purple to 0,94 for the red edge band. The UHSR topobathymetry has been mapped by merging the topography and the bathymetry, distinctly predicted by the combination of the DSM with the UHSR Superdove imagery (R^2_{test} of 0,68 and 0,92, respectively).

1. Introduction

1.1 Topobathymetry Knowledge

Topobathymetry constitutes the study of the seamless terrain, either terrestrial or maritime along the coastal area (Collin et al., 2018). That discipline is underpinned by the precise and accurate measurement of the seabed and landform, both planimetrically and vertically. The terrestrial part of those interfaces is satisfactorily represented because of the dense settlement of humans and assets, necessitating reliable survey based on satellite RaDAR and aircraft infrared LiDAR (James et al., 2024). However, the maritime realm, beginning under the shoreline, has not received such attention given the cost-ineffectiveness of the airborne green LiDAR and waterborne SoNAR, compared to the land instruments. Consequently, only 15% of the worldwide lakes, rivers, streams, seas and oceans have been surveyed by reliable technology, such as active SoNAR and LiDAR (Wölfl et al., 2019).

That paucity considerably impedes the understanding and the management of the riverine and coastal risks, along with the biodiversity erosion, in the context of increasing hazards (seaward wave, landward precipitation, and sea-level rise) and growing exposure (human population) (Firth et al., 2016).

1.2 Topography Mapping

The topography can be collected at surface dimensions using the satellite and aircraft platforms. The spaceborne missions have been successful for deriving altimetry using stereo-photogrammetry (Advanced Spaceborne Thermal Emission and Reflection Radiometer, ASTER), radagrammetry (Shuttle Radar Topography Mission, SRTM), and lasergrammetry (Ice, Cloud and land Elevation Satellite, ICESat) (Yue et al., 2017).

The airborne sensors can be manned or unmanned.

1.2.1 Manned Airborne Vehicle (MAV): The MAV topographic lasergrammetry consists of the state-of-the-science to quantify the sub-meter coastal topography using a scanner laser, emitting and receiving in the infrared, either near, around 1000 nm, or mid, around 1500 nm (Helias et al., 2025).

1.2.2 Unmanned Airborne Vehicle (UAV): The recent LiDAR miniaturization enables to carry out UAV inspections to measure the land terrain with a sub-decimeter resolution (Collin et al., 2025). The UAV has been also promising to derive digital surface then terrain models from structure-of-motion photogrammetry (Mury et al., 2019).

1.3 Bathymetry Mapping

The bathymetry retrieval can be spatially modelled using spaceborne, airborne and waterborne sensors.

1.3.1 Satellite: The radiative transfer modelling is an analytical-empirical methodology to estimate the water depth from satellite using multispectral imagery, such as Sentinel-2 at 10 m (Collin et al., 2016), SuperDove at 3 m (Collin et al., 2023a), or Pleiades Neo at 0,3 m (Collin et al., 2023b).
Another robust spaceborne methodology draws on the green laser that was initially launched to measure ice topography but was harnessed to reckon shallow water depths such as lakes or lagoons (Le Quilleuc et al., 2021).

1.3.2 Aircraft

Aircraft: The MAV laser bathymetry relies on the active emission and reception of a blue (Peng et al., 2025) or green (Caline et al., 2022) wavelength (around 500 nm) to assess the shallow water depths. In addition, the UAV bathymetry mapping can be derived from the photogrammetry (Collin et al., 2024) or lasergrammetry (Mano et al., 2020).

1.3.3 Boat

Boat: The first and still in force technique to measure the bathymetry is based on the active emission and reception of sound at various frequencies, namely the sonargrammetry (Le Quilleuc et al., 2023). Recently, waterborne LiDAR systems have been revealed efficient to optically render the shallow seabed in 3D (Nakagawa et al., 2025).

1.4 Topobathymetry Mapping through Satellite-UAV Fusion

The proposed research study aims to create an innovative topobathymetric model at ultra-high spatial resolution (UHSR), that is to say < 0,1 m pixel size, from the fusion of a UAV red-green-blue (RGB) full-frame camera imagery and a satellite multispectral SuperDove imagery. That original purpose will be developed for a tropical fringing reef coast in Martinique (Figure 1), and will result from a three-step approach: (1) the fusion of the UAV RGB and satellite multispectral imageries comparing linear and nonlinear regression algorithms, (2) the UHSR topography modelling comparing linear and nonlinear regressors trained with a third-party MAV topographic LiDAR, and (3) the UHSR bathymetry modelling comparing linear and nonlinear regressors trained with a third-party MAV bathymetric LiDAR.

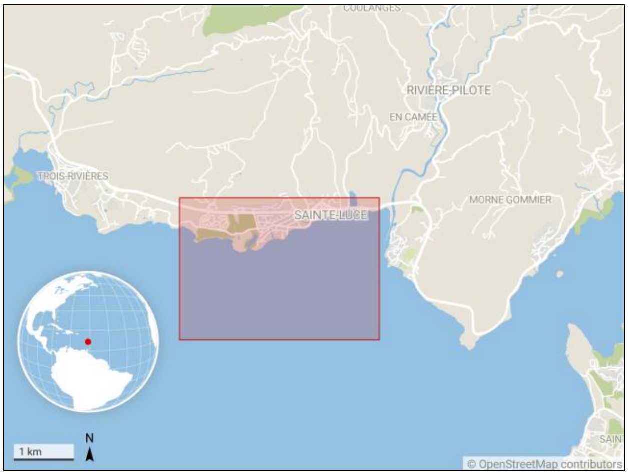

Figure 1. Location map of the study site (*Gros Raisins*’ Beach, Sainte-Luce, Martinique Island, France).

2. Methodology

2.1 Study Site

The land-sea continuum, where took place the proof-of-concept of that research, consists of a coral reefscape tied to the beach of *Gros Raisins* (14°46’N, 60°93’W), along the coast of Sainte-Luce city, in the Martinique Island (France), belonging to the Lesser Antilles. That hybrid area of terrestrial and marine realms extends over 3,3 km^2, and hosts representative tropical habitats, such as forests, lawns, buildings, roads, beaches, seagrasses and coral reefs.

2.2 UAV Imagery

The ultra-high spatial resolution UAV collection was operated with a DJI Zenmuse P1 mounted on a DJI Matrice 300 RTK multirotor (Figure 2) on the 30th March 2024. The full-frame camera can acquire RGB bands with a focal of 2,8 and a lens of 24 mm (8192 × 5460 pixels).

Figure 2. The RGB full-frame camera (DJI Zenmuse P1) mounted on a multirotor (DJI Matrice 300 RTK).

The UAV flight comprised 220 photographs whose collection was constrained by two criteria of the planning flight: 80% and 70% for the front and side overlapping, respectively. The accuracy and precision were ensured by the third-party DJI D-RTK2 base antenna, whose xyz coordinated were rigorously reckoned with a third-party GNSS-RTK receiver, namely the Emlid Reach RS2+, linked with the Teria network. The planimetric datum was the WGS84 projected with a UTM 20N, and the altimetric reference was the IGN87.

The photogrammetry procedure has been implemented in the software DJI Terra, following aero-triangulation, tie point detection, and point cloud creation. Two raster by-products were then derived at 0,08 m pixel size from the point cloud trigonometry and attributes: a RGB orthomosaic (Figure 3) and a land-sea digital surface model (DSM) (Figure 4).

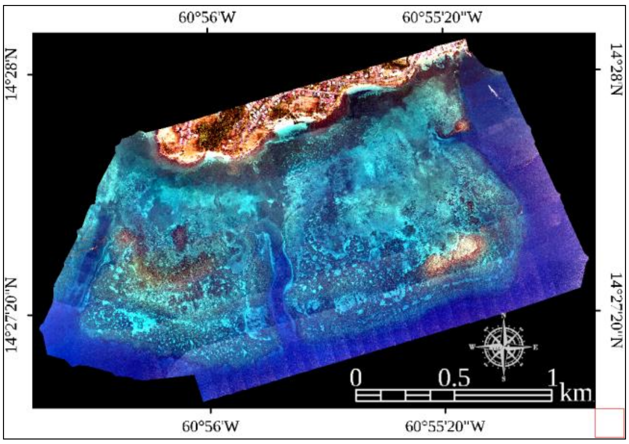

Figure 3. Natural-colored map UAV of the study site (*Gros Raisins*, Martinique Island, France) derived from the survey based on the DJI Zenmuse P1 mounted on a DJI Matrice 300 RTK (30th March 2024).

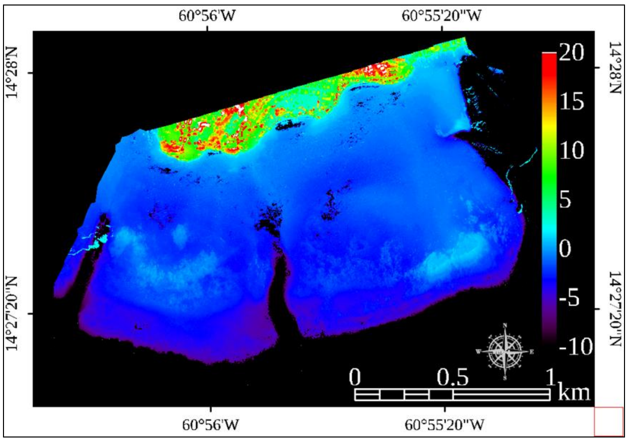

Figure 4. Digital topobathymetric surface model of the study site (*Gros Raisins*, Martinique Island, France) derived from the survey based on the DJI Zenmuse P1 mounted on a DJI Matrice 300 RTK (30th March 2024).

2.3 PlanetScope SuperDove Imagery

The multispectral imagery was stemmed from the third and last constellation of the PlanetScope nanosatellites, named SuperDove imagery (PSB.SD, 10 cm × 10 cm × 30 cm, Figure 5).

Figure 5. The spaceborne multispectral SuperDove nano-satellite CubeSat (Planet Labs).

Orbiting between 475 and 525 km since 2020, the SuperDove CubeSats provide six visible (purple or Coastal Blue, blue, green 1, green, yellow, red) and two near-infrareds (red edge and near-infrared) whose centered wavelengths reach 441, 490, 531, 565, 610, 665, 705 and 865 nm, respectively (Table 1).

Band number	Band name	Wavelength Min. (nm)	Wavelength Max. (nm)
1	Purple or Coastal Blue	431	452
2	Blue	465	515
3	Green I	513	549
4	Green	547	583
5	Yellow	600	620
6	Red	650	680
7	Red Edge	697	713
8	Near-Infrared	845	885

Table 1. PlanetScope SuperDove spectral specifications.

The average spectral resolution of the eight bands attains 31 nm, ranging from 15 nm for the red edge to 50 nm for the blue bands. The spatial resolution is high with a 3 m resampling size, while the temporal resolution is very high since daily (Collin et al., 2023a).

The satellite imagery was collected on the 31st March 2024 at 13h53min08sec UTC, that is to say one day after the UAV survey. The imagery was selected based on three filters on the Planet on-line platform: 100% of the area coverage, <10% of the cloud cover, and the closest day of the UAV campaign. Once chosen, the imagery was geometrically corrected under that projected datum: WGS84 / UTM 20N. It was then radiometrically corrected at the bottom-of-atmosphere surface reflectance in order to compensate for the light-atmosphere interactions and to account for the sun irradiance (Figure 6).

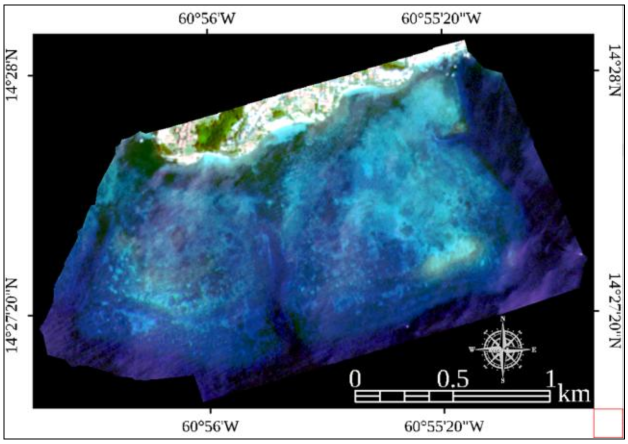

Figure 6. Natural-colored map of the study site (*Gros Raisins*, Martinique Island, France) derived from the PlanetScope SuperDove acquisition of the 31st March 2024.

2.4 LiDAR Data

The study area was previously monitored using a topobathymetric airborne LiDAR system in 2010 and 2011 by the French Navy (open source: https://diffusion.shom.fr/litto3d-mart2016.html). The LiDAR point cloud was rasterized at 0,08 m pixel size (WGS84 / UTM 20N - IGN87, Figure 7) to match the scale of the UAV RGB orthomosaic and land-sea DSM.

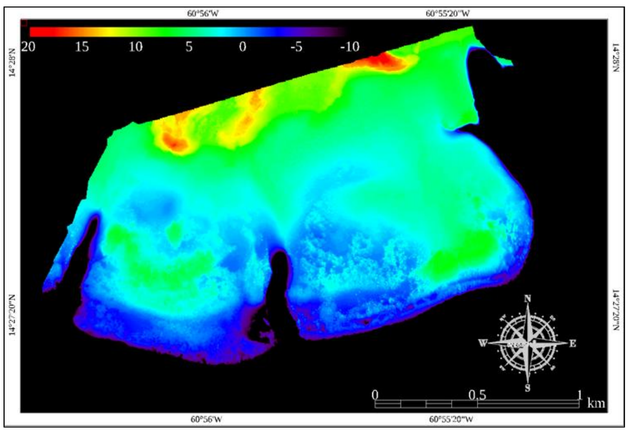

Figure 7. Digital topobathymetric terrain model of the study site (*Gros Raisins*, Martinique Island, France) derived from the survey based on the airborne LiDAR of the product Litto3d® Martinique 2016.

2.5 Spatially-Explicit Modelling

2.5.1 UAV-Satellite Fusion: The first objective of the research was to merge the DJI Zenmuse P1 with the PlanetScope SuperDove to get eight spectral bands at 0,08 m. First, an array of nine representative habitat classes provided with spectral characteristics was associated with both imageries: deep sea, coral reef, reef flat, seagrass, shallow sand, beach, grass, tree, and roof. Second, a series of 99 pixels for each habitat class was sub-divided into 33 calibration, 33 validation and 33 test sub-datasets. Two types of regressions were run and compared: linear and nonlinear; the last one in the form of a shallow neural network; composed of two hidden layers with three neurons, each. The three bands tied with the UAV survey consisted of the predictors trained to model each response of the eight SuperDove bottom-of-reflectance bands (Figure 8). Once the best formula was found out for each SuperDove band, it was applied at the UAV scale to obtain a multispectral imagery at UHSR.

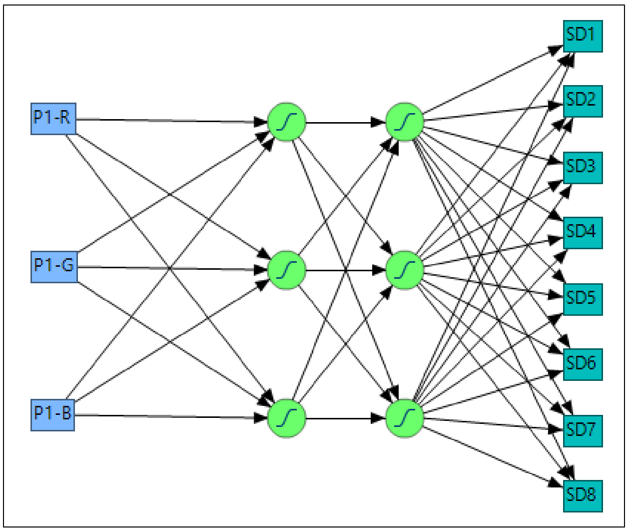

Figure 8. Neural Network regression linking the three UAV predictors (RGB from the DJI Zenmuse P1) with the eight satellite responses (PlanetScope SuperDove, SD).

2.5.2 Topobathymetry Modelling: The second main objective was to model the topobathymetry at 0,08 m. On the one hand, the UHSR topography was modelled using the topographic part of the LiDAR as the response. Once the UHSR SuperDove imagery along with the photogrammetry-based land-sea DSM was stacked with the LiDAR raster, 179 758 pixels, ranging from -0,20 m to 17,69 m elevation (IGN87), were equally and randomly sub-divided into 59 919 pixels for the calibration, validation, and test sub-datasets, each. On the other hand, the UHSR bathymetry was modelled using the bathymetric part of the LiDAR as the response. A total of 124 696 pixels, ranging from -10 to 0,2 m elevation (IGN87), were also evenly split into three pools: 41 565 pixels for the calibration, validation and test sub-datasets, each. Like for the fusion modelling, two families of regressions were implemented and compared: the linear regression and the neural network regression (two hidden layers provided with three neurons each). Furthermore, three categories of predictors were tested: the land-sea DSM, the land-sea DSM + visible UHSR SuperDove imagery, and the land-sea DSM + optical USHR SuperDove imagery.

3. Results and Discussion

3.1 UAV-Satellite Fusion

3.1.1 Linear Regression: The performance of the linear modelling the predict the eight SuperDove bands by the three RGB UAV bands was satisfactory, even very satisfactory (Figure 9A), with the least score attributed to the blue band (R^2_{test}=0,68), and the best achievement associated with the red band (R^2_{test}=0,81).

3.1.2 Neural Network Regression: The nonlinear approach to fuse the satellite imagery at the UAV scale yielded much better outputs than the linear regression (Figure 9B). The least performance indeed bottomed with the purple band (R^2_{test}=0,79) and topped with the red edge band (R^2_{test}=0,94).

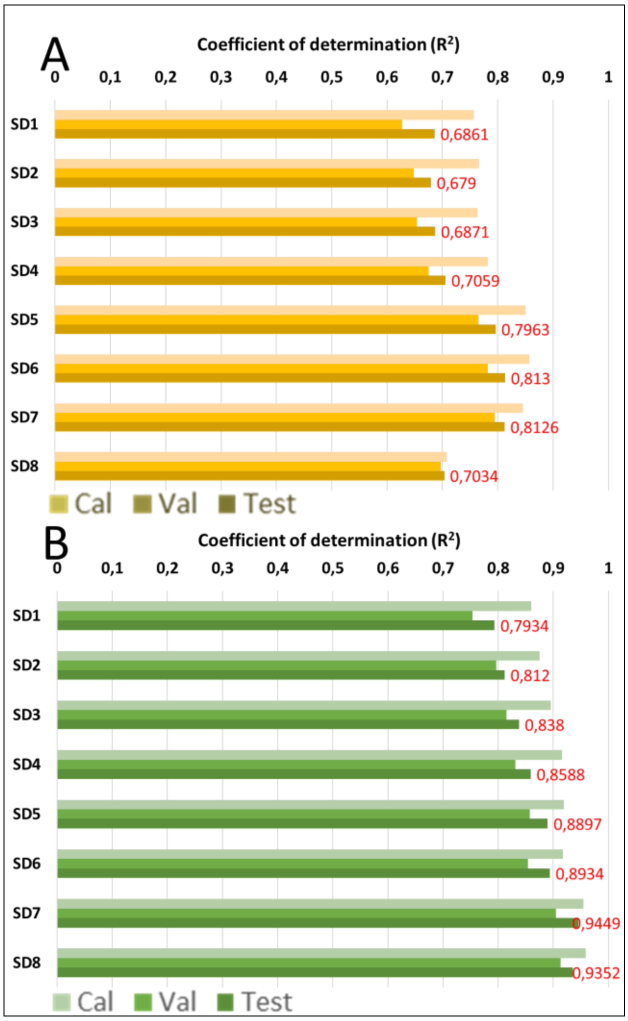

Figure 9. Histogram performance of the UAV-satellite fusion for (A) the linear, and (B) the neural network prediction of the eight SuperDove (SD) bands by the RGB P1 UAV imagery.

The findings derived from the neural network modelling were logically chosen at the detriment of the linear results. For each of the eight SuperDove bands, the mathematical formula, constructed on the neural network architecture, was applied with a raster calculator at the original UAV orthomosaic in order to handle the UHSR SuperDove imagery (Figure 10).

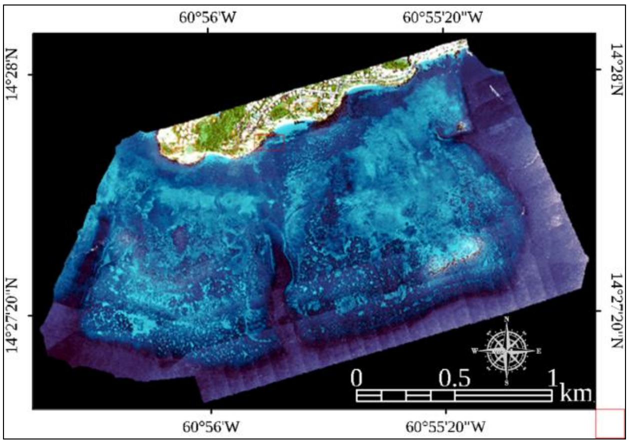

Figure 10. Natural-colored UHSR UAV-satellite fusion map of the study site (*Gros Raisins*, Martinique Island, France) derived from the prediction of the PlanetScope SuperDove satellite imagery (collected on the 31st March 2024) by the P1 RGB UAV imagery (acquired on the 30th March 2024).

3.2 UHSR Topobathymetric Modelling

3.2.1 UHSR Topography Modelling: The score comparison of the three datasets of linear predictors revealed that the addition of the UHSR SuperDove imagery increased the photogrammetry-based DSM by 0,1 (R^2_{test}=0,52 vs R^2_{test}=0,42). That gain was quantified as a constant, either with the visible or the optical part of the UHSR SuperDove imagery (Figure 11A). The findings tied to the nonlinear experiments showed that the combination of the optical SuperDove imagery with the DSM (R^2_{test}=0,68) brought the best score, compared to the sole DSM predictor (R^2_{test}=0,54) (Figure 11B).

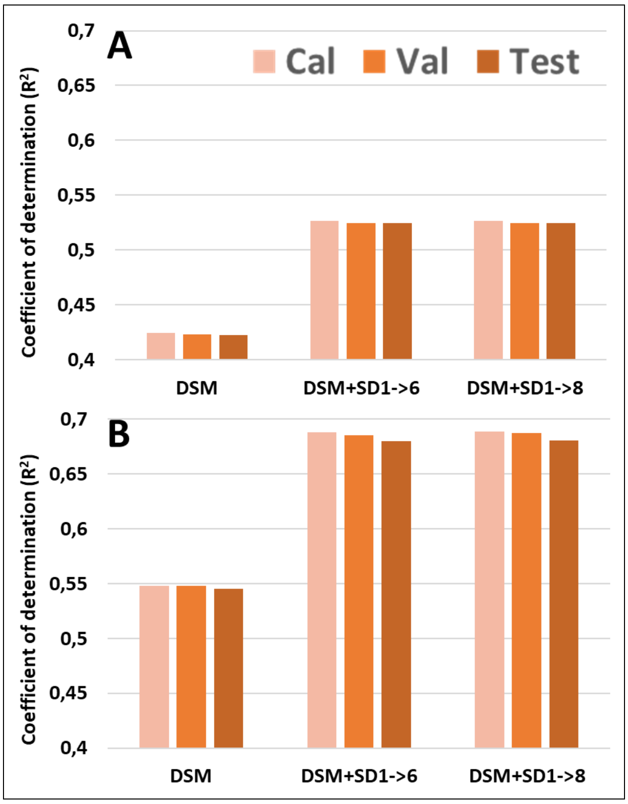

Figure 11. Histogram of the topography prediction by the (A) linear, and (B) neural network regression based on the UAV-satellite fusion imagery.

Even if the clustering of the UHSR SuperDove imagery with the DSM produced satisfactory modelling of the topography, it is important to remark that the LiDAR response was strictly restrained to the bare ground, without the above-ground elements, as detected by the photogrammetry procedure. That unneglectable discrepancy could be improved by the creation of a UAV Digital Terrain Model (DTM), instead of the DSM.

3.2.2 UHSR Bathymetry Modelling: Either linear or nonlinear, the bathymetry prediction was much better than that of the topography (Figure 12A and B). About the linear approach, the three datasets of predictors generated R^2_{test} reaching 0,86, for the sole DSM and the boosted DSM by the UHSR SuperDove imagery (Figure 12A). That excellent performance underlined the data matching of the underwater photogrammetry-derived DSM and the LiDAR DTM. The UAV bathymetric DSM can indeed be considered as a DTM, given the absence of any built-up features, encountered on land. The nonlinear technique increased the single DSM prediction by 0,01 (from R^2_{test} = 0,86 to 0,87). Contrary to the linear regression, the addition of the visible and optical UHSR SuperDove imagery to the DSM strongly augmented the neural network performance, reaching R^2_{test} = 0,91 and 0,92, respectively (Figure 12B).

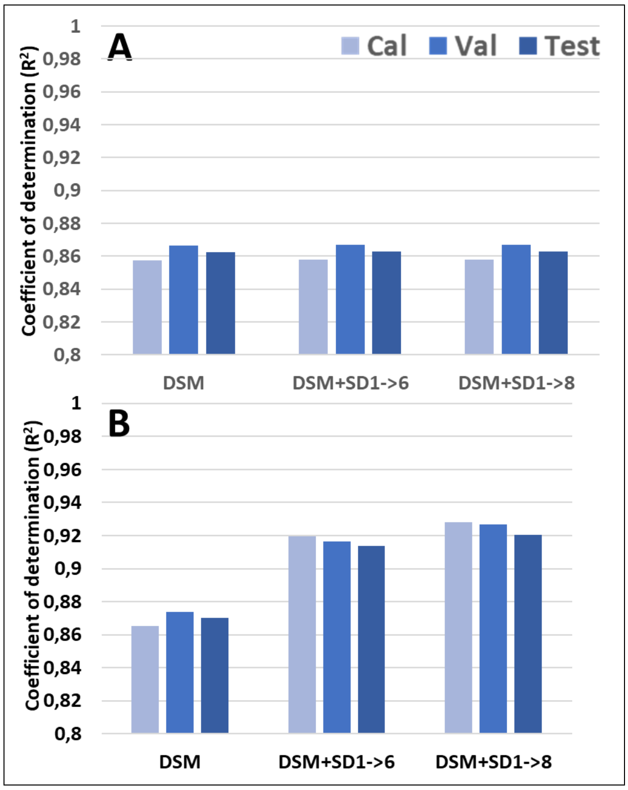

Figure 12. Histogram of the bathymetry prediction by the (A) linear, and (B) neural network regression based on the UAV-satellite fusion imagery.

3.2.3 Topobathymetry Mapping: The best combinations in terms of predicting, on the one hand, topography, and on the other hand, bathymetry, were stitched to create the UHSR topobathymetry (Figure 13). In both cases, the combination of the DSM and the optical UHSR SuperDove imagery were selected to train the neural network regression.

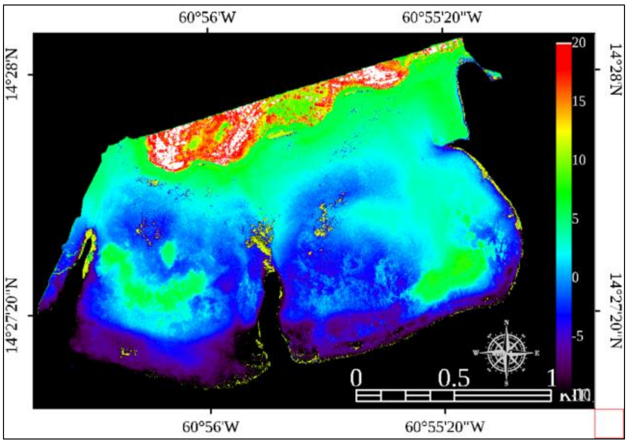

Figure 13. Digital topobathymetric surface model of the study site (*Gros Raisins*, Martinique Island, France) derived from the combinations of the DSM + UHSR optical SuperDove imagery trained by the LiDAR DTM for both topography and bathymetry.

4. Conclusions

The fusion of the DJI Zenmuse RGB P1 mounted on a UAV with the PlanetScope SuperDove multispectral satellite imagery enabled to produce a eight-band imagery at 0,08 m, that is to say at ultra-high spatial resolution (UHSR). That fusion was the most efficient with a bandwise neural network, ranging from R^2_{test} of 0,79 for the purple to 0,94 for the red edge band.

The topobathymetry mapping has been modelled at UHSR by stitching the topography and the bathymetry, whose spatially-explicit modelling was separated. Both models were based on the photogrammetry-based digital surface model combined with the UHSR Superdove imagery, that was trained on a topobathymetric LiDAR response (R^2_{test} of 0,68 and 0,92, respectively).

Acknowledgements

The authors would like to thank the French *Laboratory of Excellence CORAIL* for the mission support (Waliwave project), and the French Navy (*Service Hydrographique et Océanographique de la Marine*) for the LiDAR open-source.

References

Caline, B., Collin, A., Pastol, Y., Letard, M., Feunteun, E., 2022: New Insights into the Shallow Morpho-Sedimentary Patterns Using High-Resolution Topo-Bathymetric Lidar: The Case Study of the Bay of Saint-Malo. In *European Spatial Data for Coastal and Marine Remote Sensing: Proceedings of International Conference EUCOMARE 2022-Saint Malo*, France, 219-222. Cham: Springer International Publishing.

Collin, A., Hench, J.L., Pastol, Y., Planes, S., Thiault, L., Schmitt, R.J., Holbrook, S.J., Davies, N., Troyer, M., 2018: High resolution topobathymetry using a Pleiades-1 triplet: Moorea Island in 3D. *Remote Sensing of Environment*, 208, 109-119.

Collin, A., James, D., Feunteun, E., 2023b: Pléiades Neo-Derived Bathymetry in Coastal Temperate Waters: The Case Study of Bay of Saint-Malo. *Environmental Sciences Proceedings*, 29(1), 68.

Collin, A., James, D., Gairin, E., Aubert, M., Daniel, Y., Feunteun, E., Dubois, S., 2025: The Spatial Network of the Largest Honeycomb Reef in the World as Revealed by an Ultra-High Resolution Lidar Drone. *Journal of Coastal Research*, 113(SI), 961-965.

Collin, A., James, D., Lamontagne, N., Hardy, R., Monpert, C., Feunteun, E., 2024: Ultra-high-resolution bathymetry estimation using a visible airborne drone, photogrammetry and neural network. *Proceedings of the XVIIIèmes Journées*, Anglet, France, 25-27.

Collin, A., Laporte, J., Koetz, B., Martin-Lauzer, F.R., Desnos, Y.L., 2016: Mapping bathymetry, habitat, and potential bleaching of coral reefs using Sentinel-2. In *13th international coral reef symposium (ICRS 2016,* 405-420.

Collin, A., Palola, P., James, D., Pastol, Y., Monpert, C., Loyer, S., ..., Wedding, L., 2023a: Superdove-modelled bathymetry using neural networks along a turbidity gradient: Bréhat, Saint-Barthélémy and Tetiaroa islands. *Int. Arch. Photogramm. Remote Sens. Spatial Inf. Sci.*, 48, 1351-1356.

Firth, L.B., Knights, A.M., Bridger, D., Evans, A.J., Mieszkowska, N., Moore, P.J., ..., Hawkins, S.J., 2016: Ocean sprawl: challenges and opportunities for biodiversity management in a changing world. *Oceanography and Marine Biology: an annual review*, 54, 189-262.

Helias, M., Bailly du Bois, P., Poizot, E., Collin, A., Bizien, A., Camus, J., ..., Gallon-Garcia, R., 2025: Tidal height normalization (THN) - a new method to study the local vertical distribution of benthic intertidal organisms. *Marine Ecology Progress Series*, 775, 1-15.

James, D., Collin, A., Gallon, R., Poizot, E., 2024 : Études de la précision altimétrique (nuage de points) des géo-écosystèmes littoraux via la photogrammétrie et la lasergrammétrie par drone aérien. *Proceedings of the XVIIIèmes Journées*, Anglet, France, 497-506.

Le Quilleuc, A., Collin, A., Jasinski, M. F., Devillers, R., 2021 : Very high-resolution satellite-derived bathymetry and habitat mapping using Pleiades-1 and ICESat-2. *Remote Sensing*, 14(1), 133.

LeQuilleuc, A., Husset, M.-C., Collin, A., Feunteun, E., 2023 : Cartographie prédictive d'un coquillage invasif via l'apprentissage automatique des données acoustiques multi-fréquentielles et vérités-terrain : *Crepidula fornicata* en Baie du Mont-Saint-Michel. In *Proceedings of the 4th merIGéo* : 165-167.

Mano, K., Sakai, K., Tachibana, K., Sakita, K., Nishiyama, S., 2020: The measurement accuracy and measurement characteristics of green LiDAR drone. *Int. Arch. Photogramm. Remote Sens. Spatial Inf. Sci*, 43, 479-483.

Mury, A., Collin, A., James, D., 2019: Morpho–sedimentary monitoring in a coastal area, from 1D to 2.5 D, using airborne drone imagery. *Drones*, 3(3), 62.

Nakagawa, M., Kubo, N., Shimizu, E., 2025: GNSS/LiDAR-SLAM with Depth Image-based Scan Matching for Waterborne Mobile Mapping. *Int. Arch. Photogramm. Remote Sens. Spatial Inf. Sci*, 48, 121-126.

Peng, C., Jamet, C., Di Girolamo, P., Dionisi, D., Li, X., Zhang, S., ..., Pan, D., 2025: Airborne blue lidar reveals the ocean's hidden biological engine in the South China Sea. *Communications Earth and Environment,* 6, 1051.

Wölfl, A.C., Snaith, H., Amirebrahimi, S., Devey, C.W., Dorschel, B., Ferrini, V., ..., Wigley, R., 2019: Seafloor mapping–the challenge of a truly global ocean bathymetry. *Frontiers in Marine Science*, 6, 434383.

Yue, L., Shen, H., Zhang, L., Zheng, X., Zhang, F., Yuan, Q., 2017: High-quality seamless DEM generation blending SRTM-1, ASTER GDEM v2 and ICESat/GLAS observations. *ISPRS Journal of Photogrammetry and Remote Sensing*, 123, 20-34.